Visualization of 3D stress tensor fields using superquadric glyphs on displacement streamlines

Mohak Patel, and David H. Laidlaw, *Fellow, IEEE*

Abstract—Stress tensor fields play a central role in solid mechanics studies, but their visualization in 3D space remains challenging as the information-dense multi-variate tensor needs to be sampled in 3D space while avoiding clutter. Taking cues from current tensor visualizations, we adapted glyph-based visualization for stress tensors in 3D space. We also developed a testing framework and performed user studies to evaluate the various glyph-based tensor visualizations for objective accuracy measures, and subjective user feedback for each visualization method. To represent the stress tensor, we color encoded the original superquadric glyph, and in the user study, we compared it to superquadric glyphs developed for second-order symmetric tensors. We found that color encoding improved the user accuracy measures, while the users also rated our method the highest. We compared our method of placing stress tensor glyphs on displacement streamlines to the glyph placement on a 3D grid. In the visualization, we modified the glyph to show both the stress tensor and the displacement vector at each sample point. The participants preferred our method of glyph placement on displacement streamlines as it highlighted the underlying continuous structure in the tensor field.

Index Terms—3D stress tensor field, visualization, glyph, glyph placement, virtual reality, user study.

1 Introduction

The field of solid mechanics concerns the study of the deformation of solid materials upon application of physical forces. Solid mechanics is vital in a range of applications such as: the study of structural strength and failure analysis in mechanical, civil and aerospace engineering [1], the design of surgical implants [2], and cell mechanics [3] in biomedical engineering, soil modeling in geomechanics [4] and deformation of materials in material science [5]. While researchers have made several advances in computational modeling and experimental techniques to solve new problems, there remains a lack of effective visualization techniques for featured mechanical tensor quantities in these studies. The visualization of these tensor quantities in tandem with existing computational simulation and experimental tools can provide domain experts with crucial insights in their research [6].

Stress and strain are the most common mechanical quantities studied in solid mechanics. Both the stress and strain are tensors with similar mathematical properties. So henceforth, while we only focus on stress visualization, the design techniques of the stress visualizations employed here readily apply to the visualization of strain as well. Stress tensors describe the force acting per unit area in a material. Mathematically, stress is a symmetric, indefinite, second-order tensor. At each point the stress tensor has six independent components which can be represented as three principal stresses (eigenvalues) in the three orthogonal principal directions (eigenvectors). Visualization of stress tensor fields is challenging because of the large amount of information that they contain, i.e., six individual components at each sample point. Thus domain experts primarily analyze tensor data using 2D plots of derived quantities [7]. The major issue with such an approach is that it does not convey all information of the tensor field. By visualizing reduced quantities, researchers may lose some of the insights that could be gained from the information-rich tensor data.

Even in the visualization community, tensor field visualization is often restricted to 2D slices of 3D data. Attempts at extending tensor visualization in 3D space have suffered from issues of occlusion and clutter, particularly in the case of glyph-based visualizations [8]. Some advances have been made in combustion turbulence studies where segmentation and region of interest highlighting are used to enhance exploration and visualization of 3D tensor fields [9], [10], [11]. However, these strategies are application specific to the spatially dense data from combustion turbulence studies, which is often not the case with stress tensor field data in solid mechanics. Stress tensor visualization has some parallels with diffusion tensor visualization [12], [13], [14]; however, stress and diffusion tensors have different mathematical properties. Hence, there is a need for tensor visualizations designed with a focus for the field of solid mechanics. Moreover, the development of most of these visualization techniques is mathematically-driven. However, it is also crucial to evaluate the effectiveness of these visualization methods with domain experts. User evaluations studies have been conducted for tensor glyphs with the context in nematic liquid crystal alignment [15] and for comparative analysis of glyph-based techniques with their applicability to cerebral aneurysms [16]. Further user studies also need to be undertaken with a focus in mechanical engineering.

In this paper, we present a glyph-based visualization for mechanical stress tensors. In particular, we first adapt superquadric glyphs to represent the stress tensor, and then

• *The authors are with the Department of Computer Science, Brown University, Providence, RI 02912.*
Email: dhl@cs.brown.edu

utilize a glyph placement strategy to visualize the evolution of tensor fields in a 3D space with emphasis on minimizing clutter and occlusion. Then, we perform user studies with domain experts to evaluate glyph design and placement strategy. The user studies compare the stress tensor visualization methods on objective accuracy measures and subjective user feedback. The results of the user study can further inform the development of effective visualization of stress tensor fields and their evaluations.

Our main contribution is adapting the current glyph-based tensor visualizations for stress tensor field visualization, and the results of a formal user study evaluating various visualization methods.

2 Background and Related Work

In this section, we relate our work to the techniques developed in the literature to visualize tensor fields, particularly with a focus on mechanical stress tensors.

2.1 Local tensor visualization

We base our work on the local method of utilizing glyphs to represent a single tensor state at discrete positions across a tensor field. A glyph is a geometric icon which allows depiction of a tensor by encoding its various parameters into properties like shape, size, and color.

2.1.1 Glyphs

Our method builds upon the foundational work of Kindlmann [17] in the development of superquadric glyphs (SQ glyphs) to visualize diffusion tensors in magnetic resonance imaging. Kindlmann's SQ glyphs combined useful features of the ellipsoid and cuboid glyphs to represent the diffusion tensor, but they were limited to only visualizing positive-definite second-order tensors. To overcome this limitation, Schultz et al. extended the superquadric glyphs (extended SQ) to depict positive-definite, indefinite, or negative-definite symmetric second-order tensors [18], at the cost of being visually more complex than SQ glyphs.

Among all of the glyphs in the literature, extended SQ glyphs appear to be the best choice for stress tensor visualization as they can illustrate all the permissible states of the stress tensor, while equally prioritizing all the principal stress components in the visualization. Also, Abbasloo et al. [19] used extended SQ glyphs in the visualization of the stress tensor, where the work addressed data uncertainty in second-order tensor fields. However, the extended SQ represents positive-definite and negative-definite tensor state with a convex glyph and the indefinite tensor state with a concave glyph. Nevertheless, all six independent components of the tensor state are already encoded in the size and color along the glyph axes and their orientation. Thus, the additional dimension of information about the signs of the eigenvalues encoded by the convexity or concavity of each glyph shape is redundant and increases the visual complexity of the extended superquadric glyph. In our method, we use simpler SQ glyphs in tandem with a diverging colormap based encoding to represent all states of the mechanical stress tensor. The color encoding makes our glyph easier to interpret and reduces the user errors in deciphering the tensor states.

In the selection of glyph for visualization in our work, we also considered other glyphs developed to represent mechanical stress tensors. We eventually did not use these glyphs because of their various limitations. For example, the Haber glyph encodes stress into a geometric combination of cylindrical and elliptical glyphs [20]. The primary limitation of this is that it only focuses on the major principal stress. The Reynold glyph encodes the normal stress in any direction through its shape and color [21]. However, the Reynold glyph is visually complex and suffers from information contraction [22]. Similar to the Reynold glyph, the HWY glyph shows shear stresses [4]. Its limitations are that it does not show the directions of shear stress, it is a nill glyph for isotropic stress direction, and it has a visually complex shape. Kratz et al. comprehensively compare the commonly used glyphs with context in mechanical engineering, motivates design of tensor glyphs based on its invariants and introduces multi-perspective visualization of the tensor fields [6], [13]. Gerrits et al. [23] proposed glyphs to account for applications requiring more general second-order tensors beyond the requirements for stress tensors.

2.1.2 Glyph placement

Tensor glyph placement approaches in 3D suffer from clutter and occlusion issues, and limitations in highlighting continuous features in the underlying tensor field. Directly placing tensor glyphs on a regular 3D grid with large spacing may decrease occlusion, but this glyph placement strategy does not show the continuous underlying structure in the tensor field and also has the visual artifacts associated with regular sampling. To display the continuous structures in the tensor field, Shimada et al. presented the work on a particle-based approach to accomplish adaptive anisotropic meshes conforming to a given tensor field [24]. Kindlmann et al. improved on this approach by utilizing the potential energy field from the tensor field to achieve dense glyph packing [25]. These approaches have been more successful in 2D compared to 3D because while they show some continuous structure in the tensor field, they do not solve the issue of clutter and occlusion in 3D. In 2016, Marai et al. [11] explored tensor glyph placement on velocity streamlines for visualization of dense tensor fields in computational turbulence studies. However, the domain experts in the research did not gain new insights from this glyph placement strategy compared to glyph placement on a 3D grid. In context of diffusion tensor visualization, glyphs have been placed on streamlines to highlight the continuous structures in the tensor field [26], [27].

The other tensor glyph placement strategy developed for 2D [28], [29], [30] focuses on dense glyph packing to show features in the tensor fields. But such methods cannot be directly extended to 3D space, as dense glyph packing in 3D space leads to occlusion and clutter. Thus, in our method, we focused on strategically and sparsely placing glyphs to avoid occlusion and reducing clutter in 3D space while showing the inherent continuous features of the underlying stress tensor field while reducing clutter and occlusion.

2.2 Continuous tensor visualization

Continuous tensor visualization methods emphasize the global structures and regional coherence of tensor fields.

Usually, these methods either show scalar or vector quantities derived from the tensor field. A comprehensive review of various continuous tensor visualization methods has been presented by Kratz et al. [8].

Our work does not belong entirely under the continuous tensor visualization methods but is instead a hybrid between local and continuous tensor visualization methods. Like traditional vector methods, we exploit the derived vector field from the tensor field in our visualization. In the literature [31], [32], [33] approaches to visualize tensorlines, streamlines of an eigenvector of a tensor field, have been used to visualize the underlying tensor field. But these methods only focus on one eigenvector. Visualization of tensorlines has been extended to hyperstreamlines [34], [35], [36] and superquadric streamtubes [37], which incorporate the other eigenvectors and eigenvalues, but due to clutter are limited to low resolution. Instead, we use streamlines of the displacement vector field to show the continuous structures of the stress tensor field.

3 METHODS

Here we present a glyph and placement design strategy for visualization of 3D stress tensor fields. We then perform user studies to evaluate our method against the current glyph based methods for stress visualization. We hypothesize that our visualization method is more intuitive to interpret and reduces user errors compared to current tensor visualization methods.

3.1 Glyph

3.1.1 Our glyph method

To represent all the states of the stress tensor, we color encoded the SQ glyph to differentiate the positive and negative principal stress values. We used a diverging red-blue colormap to show both the sign and the magnitude of the principal stresses as shown in Figure 1. The red colored and blue colored portions of the colormap indicate positive and negative principal stresses respectively.

The color encoding process is detailed as follows. First, we computed the Euclidean distance of each point on the glyph surface to points on the glyph surface intersecting with the principal directions. The set of points having the smallest distance for a particular principal direction were assigned to it, and colored to encode the corresponding principal stress value, as similarly done by Schultz et al. [38]. The distances assigned to each principal direction were linearly normalized between 0 and 1. Assume a point having a normalized distance d to its principal direction with a stress value of σ. For this point, its principal stress value was transformed to $\sigma(1 - d^4)$ and was then color encoded from the diverging red-blue colormap.

3.1.2 Glyph user study

We designed user tasks to evaluate participant accuracy in determining the principal stresses and directions and the subjective feedback for each glyph method.

As user tasks, subjects were shown a range of stress states for each glyph method on a traditional desktop screen. For each glyph, subjects estimated all the principal stresses and directions in a Matlab GUI. We estimated user accuracy by computing absolute principal stress error and principal direction error. The absolute principal stress error (σ_e) is defined as, $\sigma_e = |\sigma_t - \sigma_u|$. Here, σ_t is the true principal stress value and σ_u is the user estimated principal stress value. The principal direction error is the angle between the true and participant estimated principal direction. The principal direction error is less meaningful for nearly isotropic stress states. However, the goal of these error metrics was for comparative analysis of the various glyph methods instead of providing absolute errors for each glyph method.

In each post-task questionnaire, we collected the subjective feedback for each glyph method. Users rated each glyph method for its mental demand, temporal demand, and user preference rating. Mental demand and temporal demand are based on the NASA-TLK scale [39]. Mental demand is defined as the mental and perceptual activity required in completion of the task. Higher values indicate that the task completion required greater mental demand. Temporal demand is defined as the time or inverse user pace required in completion of the task. Higher values indicate the task required more temporal demand, or that the participant had a slower pace in task completion. For user preference rating, participants rated the method on a seven-point Likert scale [40]. Higher values indicate a greater preference for the glyph.

3.1.3 Glyph conditions

In the user task, we compared our red-blue colored SQ glyph against a baseline of the extended SQ glyph. To isolate the differences produced by a change in shape and change in color encoding, we added an intermediate condition where we only changed the color encoding of the extended SQ glyph to the red-blue color encoding. Hereafter, we will use the following abbreviations for the glyph methods: A = extended SQ glyph; B = red-blue color encoded extended SQ glyph; and C = red-blue color encoded SQ glyph. Overall, we performed glyph accuracy user study on three conditions: A as a baseline condition or control; B as an intermediate condition; and C as our glyph method (see Figure 1).

3.1.4 Glyph dataset

Each task consisted of a visualization method paired with the same set of stress tensor data across tasks. In our pilot studies, we found accuracy and difficulty of the task to be a function of the dataset, and thus we ensured that participants saw the same set of stress tensor data for each visualization method. We carefully generated nine stress states in the dataset to cover the range of principal stress value and direction combinations. The set of stress states were normalized to have minimum and maximum principal stress value to be between -1 and 1. As discussed earlier, the principal direction error is ill-defined for nearly isotropic cases. However, only one of the nine stress state in the test was close to an isotropic tensor state. As such the deficiency of the error metric will have minimal influence on the user principal direction estimation error in the trial. We then generated an additional three stress tensor states to be used for participant training. The details of tensor states

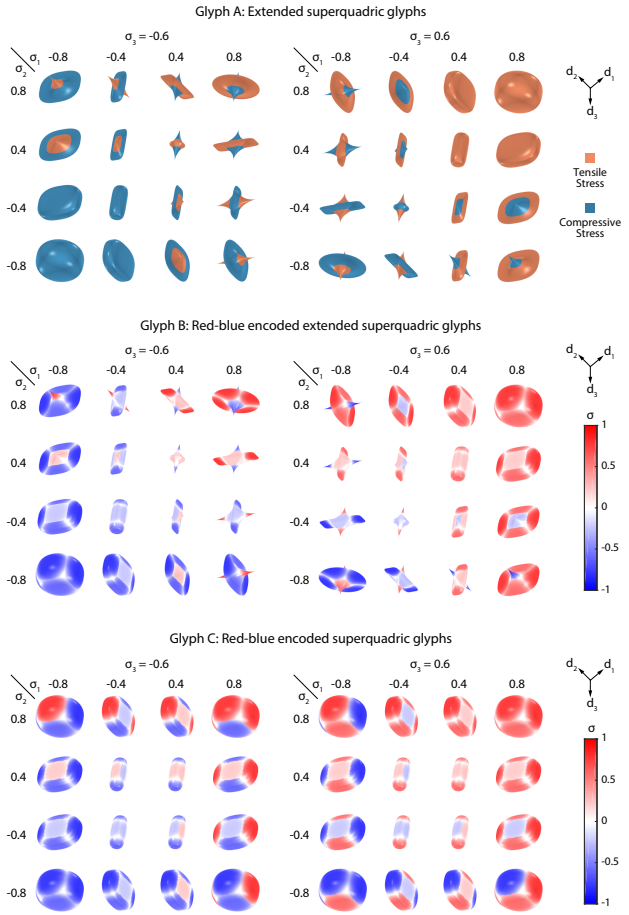

Fig. 1. Glyph methods used as conditions in the glyph evaluation trial. σ_1, σ_2 ,and σ_3 denote the principal stresses, and d_1, d_2, and d_3 denote the principal directions.

used in training and testing are described in Supplementary Information.

3.2 Glyph placement strategy

3.2.1 Our glyph placement method

Our method places stress tensor glyphs on 3D displacement streamlines. This glyph placement approach shows the inherent continuous structures of the underlying stress tensor field while sparsely placing glyphs to avoid clutter in 3D space.

Displacement field has a direct physical meaning connected with both stress and strain in mechanical engineering. A displacement field precisely describes the motion of each point in a solid. And a strain field is a deformation measure describing the ratio of deformation or displacement of a point in a solid relative to its original length. Additionally, the constitutive material properties of the solid define the relationship between the stress and strain fields. Thus, we exploit the inherent connection of the displacement field with the stress and strain fields in the visualization of the stress or strain tensor field. However, the displacement field can also have a rigid body motion component, which does not contribute to the material deformation or the material stresses. Thus, we remove the rigid motion components

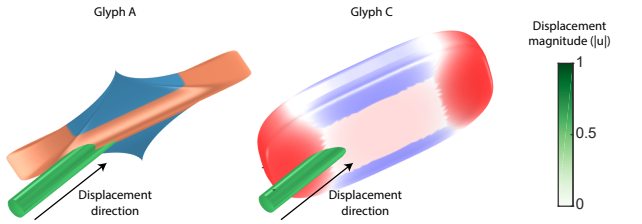

Fig. 2. A combined glyph showing both the local stress state tensor and displacement vector at a discrete location.

from the displacement fields in the visualization. Henceforth, the usage of the term displacement field refers to the displacements having no rigid body motion components.

Streamlines are useful in the visualization of displacement fields. In our visualization, we generate streamlines from random points in 3D space with a constraint on the minimum separation distance between two streamlines. The glyphs are placed on these streamlines with a constant glyph center-to-center spacing between glyphs and along the streamline. We modify the glyph to show both the local stress tensor and displacement vector as shown in Figure 2. Rods are used to describe the displacement vector. The length and color of the rod indicate the magnitude of the displacement vector. The displacement vector points along the axis of the rod towards the tensor glyph. In our visualization, the user can observe both the displacement and the stress tensor field at the same time.

3.2.2 Glyph placement user study

We used insight-based evaluation to compare the visualization methods [41]. Our tasks aimed at testing how well participants understand the stress tensor and displacement field for each visualization method. Experts in solid mechanics look for different scientific features in a stress tensor field depending on the given scientific problem. According to our best general description for solid mechanics experts intention, they are all trying to find regions of stress concentrations or high stress values, and understanding the variation of stress tensor around such concentrations. We developed tasks to capture the accuracy of subjects in identifying such features and gaining insights into the stress and displacement field. As a user task, subjects were shown coupled stress and displacement fields in virtual reality (VR) for each visualization. Subjects had to find stress and displacement insights in each visualization method.

Participant tasks and the scoring system for the stress insights were:

- Find local tensile and compressive principal stress maxima (one point for each maxima found). These stress values can be in any principal direction.
- Find the absolute maximum principal stress (one point for each maximum found). These stress values can be in any principal direction.
- On the previously found absolute maximum principal stress, determine the relative magnitude of principal stresses and principal direction on the same glyph (one point for each principal stress and direction pair).

- Describe the local variation of all three principal stresses and directions around the previously identified glyph (one point for each principal stress and direction pair variation).

Participant tasks and the scoring system for the displacement insights were:

- Find the local displacement magnitude maxima (one point for each maxima).
- Find the maximum displacement magnitude (one point for each maximum).
- In the previously identified point, find the direction of the displacement vector (one point).
- Draw two displacement streamlines starting from two different local displacement magnitude maxima (one point for each streamline).

Through these user tasks, we recorded the stress and displacement insight errors, which are defined as the ratio of total incorrectly and unidentified insights to the total number of true insights in the visualization. In the post-task questionnaire, we record user mental demand, temporal demand, and user preference rating, as previously defined in section 3.1.2, for each visualization method.

3.2.3 Glyph placement conditions

In the user task, we aim to compare displacement streamline glyph placement against 3D grid glyph placement coupled with the choice of the tensor glyph (see Figure 3). Hereafter, we will use the following abbreviations for the visualization methods conditions used in the user tasks: *AG*: glyph A on a 3D grid; *CG*: glyph C on a 3D grid; *AS*: glyph A on displacement streamline, and *CS*: glyph C on displacement streamline. All tested visualization methods also have the same displacement rod glyph attached to the tensor glyph as discussed earlier.

3.2.4 Glyph placement datasets

Each trial consisted of a visualization method and a dataset pairing. In our pilot studies, we found the user accuracy performance correlated with the dataset. However, the nature of the tasks meant that using the same dataset for each visualization would lead to user memorization of task answers. We wanted to avoid such a scenario, thus each visualization method had different but similar kind of tensor field.

For each visualization method, we showed the subjects two types of tensor fields. In the first type of the tensor field, using FEniCS, we simulated Gaussian traction fields applied on the top surface of a cuboidal solid. We varied the number, location, amplitude, and standard deviation of the Gaussian traction boundary condition for each visualization method. For the second type of tensor field, we used an analytical solution of the Eshelby inclusion problem [42], [43] where an eigenstrain is applied to a spherical inclusion in an infinite elastic body. In the visualization, we showed the tensor field in a cubic region cropped around the spherical inclusion. For different visualization methods, we changed the eigenstrain applied to the spherical inclusion. Overall, the user trial involved two tensor field datasets for the four different visualization methods. The details of the tensor field dataset generation is provided in Supplementary Information.

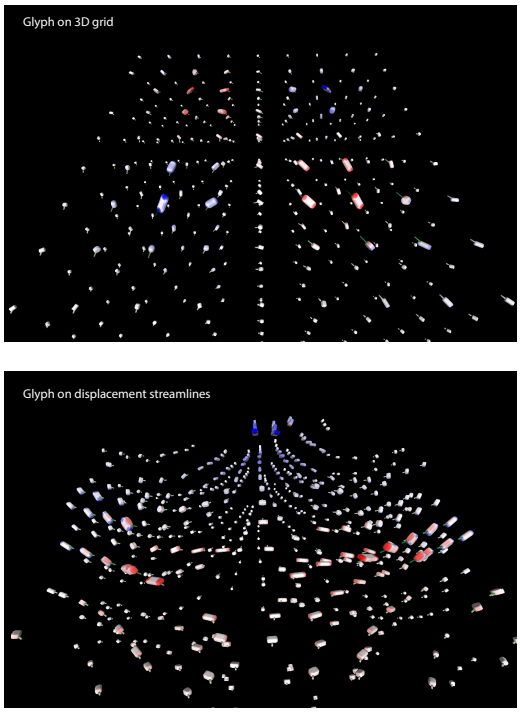

Fig. 3. Glyph placement strategy for glyph C. *Top*: Glyphs placed on a 3D grid. *Bottom*: Glyphs placed at displacement streamlines with a constant distance between them along the streamline (see Supplementary Information and Supplementary Video 1).

4 Experimental Details

4.1 Experimental Design

In the glyph evaluation experiment, we used a 3x9 within-subject design, i.e., each subject saw every experimental condition with the following independent variables: glyph (A, B, and C), and test cases (9 stress tensor states).

In the glyph placement evaluation experiment, we used a 2x2x2 within-subject design with the following independent variables: glyph (A and C), glyph placement (on a grid and on displacement streamline), and test cases (2 different tensor fields).

All the tasks for each experiment were completed in series. We used Latin squares to randomize the ordering of visualization methods within each trial to counteract the order effects in the experimental results.

4.2 Hypotheses

Our hypotheses were:

- In glyph methods, glyph C would perform the best in terms of user accuracy and subject feedback in determining the state of stress tensor.
- Glyph placement on streamline would outperform placing glyphs on a 3D grid and glyph C will outperform A in tensor field visualization.

4.3 Apparatus

The glyph evaluation experiments were performed on traditional desktop monitor (ASUS model VE278Q, 1980x1080

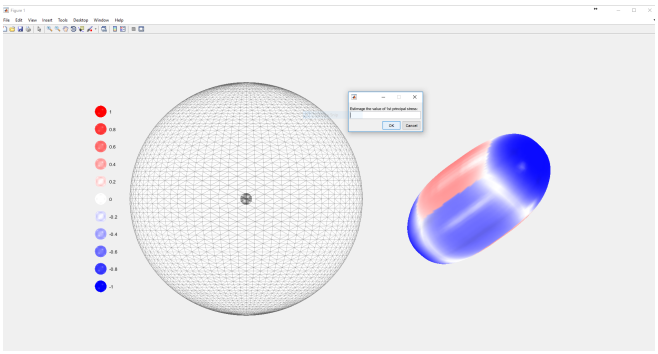

Fig. 4. Matlab GUI for conducting glyph evaluation user trial. A glyph representing a stress state is shown on the right, colormap and size estimator on the left, and sphere on which subjects estimate principal directions is on the center.

resolution, 27 inch wide) and using standard mouse and keyboard. Monitor, keyboard, and mouse were kept on a desk and participants sat on a chair with a viewing distance of about 2 feet away. Participants were free to adjust the height of the seat and distance from the desk. Participants performed the glyph evaluation trials on a Matlab GUI.

We conducted the glyph placement evaluation experiments in VR. We generated the visualization using HTC VIVE VR system which was powered by Unity software. Participants wore the HTC VIVE VR headset (1080 x 1200 resolution per eye, 110 degrees field of view and 90 Hz refresh rate) and held HTC VIVE controller in each hand to interact with the visualization. The VR system was set up in a 13 by 10 feet moving area for the participants. Two base stations, placed diagonally across the moving area, were used for motion tracking.

4.4 User interaction

In the glyph evaluation task, participants used a mouse and keyboard to interact with a Matlab GUI (see Figure 4) to estimate the principal stress values and directions for a given glyph. A glyph, representing a stress state for the trial, is shown on the right in the GUI. Users use the colormap and glyph size estimators on the left in the GUI to estimate the principal stress values. In a dialog box, participants log their estimation for a particular stress value. Participants then estimate the corresponding principal direction by clicking a point on the surface of the sphere located in the center of the GUI. In this task, participants need to select the point on the sphere surface at which the principal direction would intersect with the surface of the sphere if the glyph were in the center of the sphere. Participants were not allowed to change the viewpoint from which the glyph was observed.

In the glyph placement user study, participants could change the scale and rotate the visualization using VR controllers. Participants first explored the visualization in VR, and then answered the ordered stress and displacement insights questions verbally and by pointing out locations using the controller. The person examining the study could observe the participant VR view on a desktop screen and logged the user results. All participants were observed by Mohak Patel.

4.5 Timing and training

Participants at the beginning of the user study completed an IRB consent form. Then, we evaluated participants mental rotation ability using the Cube Comparison Test from the ETS Kit of factor-referenced cognitive tests [44]. We then explained a glyph method to the participants and trained the participants in the GUI environment and glyph method with the three training tensor states for each visualization method. Participants next completed the corresponding glyph method evaluation trial. On the completion of each task for all glyph methods, participants provided subjective feedback on the glyph method in the post-task questionnaire and debriefing session. This process was repeated for the remaining two glyph methods.

Glyph placement trials followed the glyph trials. We explained participants the glyph placement methods, and stress and displacement insight questions for the glyph placement evaluation task. The participants were then trained on using the controller to interact with the visualization environment. Following the training, participants completed the glyph placement trials.

The user training before the test evaluation ensured that short-term learning effects were minimized. However, our user study design cannot measure long-term learning effects. Designing user studies to evaluate the long-term learning effects will be insightful to explore in future studies.

At the end of each task, participants provided subjective feedback for the method in post-task questionnaire and debriefing sessions. At the end of the trial, participants provided their background information. Each study trial took on average about 2 hours and participants were given breaks between the tasks.

4.6 Participant pool

Two female and ten male subjects participated in the study. The mean age of the participants was 25 years. Subjects were drawn from two mechanical engineering undergraduate students, one material science doctoral student, three biomedical engineering doctoral students and six solid mechanics engineering doctoral students. Before completion of the user study, seven participants had no VR experience, four subjects had experienced VR once, and one subject had experienced VR multiple times. All subjects participated in all the possible combinations trial conditions for the user study.

4.7 Statistical Tests

The study used within-subject factors to compare the stress visualization methods. To compare visualization methods or treatments for statistically significant differences, we used one-way repeated measures analysis of variance (One Way RM ANOVA) if the treatment data satisfied the Shapiro-Wilk normality test with $p < 0.05$. If the treatment data failed the Shapiro-Wilk normality test, we used Friedman repeated measures analysis of variance on ranks (RM ANOVA on ranks) for comparing treatment differences. For all pairwise multiple comparisons we used the Student-Newman-Keuls post-hoc test. The differences were considered to be statistically significant if $p < 0.05$. Hereafter, all uses of the word

TABLE 1
Statistics for glyph visualization method comparisons. DOF is the degree of freedoms in the χ^2 statistic.

Comparison across all glyph methods	F	χ^2	p
Median principal stress	-	12.0; 2 DOF	0.002
Median principal direction	-	15.7; 2 DOF	<0.001
Mean mental demand	23.0	-	<0.001
Mean temporal demand	14.8	-	<0.001
Mean user preference	20.6	-	<0.001

"significantly" refers to statistically significant differences. The statistical tests were performed using SigmaPlot 12.0.

5 Results

In the study, we found a consistent trend in the objective user performance metrics and the subjective user feedback for the visualization methods. Participants had the highest accuracy in determining the state of stress using glyph B and glyph C. In the subjective feedback, participants most preferred method was glyph C. In terms of glyph placement strategy in visualization of the stress and displacement fields in a 3D volume, CS performed best in both objective and subjective metrics. The comparison results are described in detail in the following subsections. Table 1 & 2 show the statistics for the various comparisons.

In the graphs, we use boxplots to visualize the distribution for each treatment. The boxplots are generated using Seaborn version 0.9.0, a Python data visualization library, with the default parameters. The boxplots show the data median, first quartile and third quartile, while the whiskers extend to show the rest of the distribution, except for points that are determined to be outliers. The dots on the boxplot plot show the raw data values. In the graphs, a statistically significant difference between two treatments is shown by a line connecting their boxplot with an annotation for the p-value. The symbols *, **, and *** represent p values of <0.05, <0.01, <0.001 for pairwise Student-Newman-Keuls post hoc test after One Way RM ANOVA. The symbol + represents p value of <0.05 for pairwise Student-Newman-Keuls post hoc test after RM ANOVA on ranks.

5.1 Glyph

In the following sections, we show user accuracy and subjective user feedback on various glyph methods to visualize the stress tensor. As before, in the graphs and discussion we use the following abbreviation for the three glyph methods: A = extended SQ glyph; B = red-blue color encoded extended SQ glyph; and C = red-blue encoded SQ glyph. Table 1 shows the statistics for the glyph visualization methods comparisons.

5.1.1 Quantitative summary

Across all tasks, participants had the highest absolute median principal stress error and median principal direction error for A, which are significantly larger than that for B and C (see Figure 5). We found no significant difference in participants estimations of principal stress and directions between B and C. We also found no significant differences between user times in completion of trials for each glyph design.

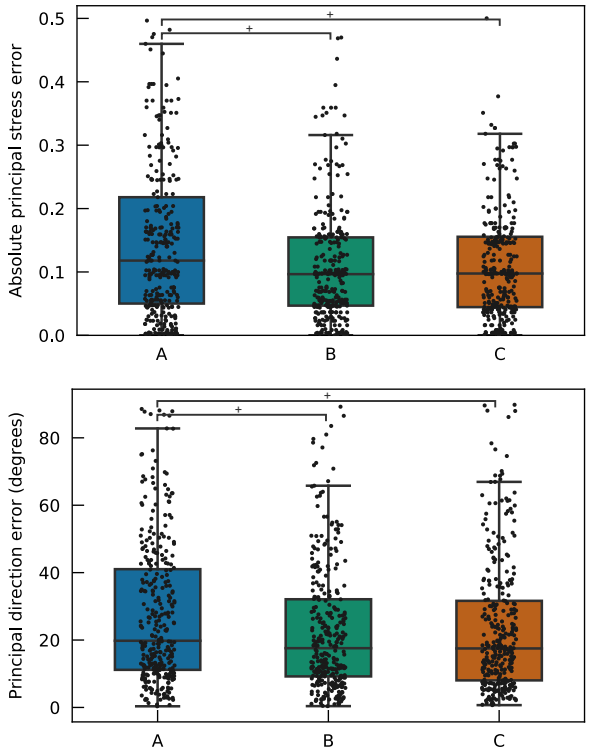

Fig. 5. Participant error in estimating the state of stress tensor. *Top:* Absolute participant error in determining the principal stress values across all glyphs. *Bottom:* Participant error in determining the principal stress directions across all glyphs. The symbol + indicates p values <0.05 for pairwise Student-Newman-Keuls post hoc test.

5.1.2 Subjective summary

In the post-task questionnaires, participants ranked A to have the highest mental and temporal demand across all methods, which was significantly higher than B, which was in turn significantly higher than C (see Figure 6). This is an interesting result since we found no significant difference between B and C in objective quantitative errors. This trend holds true in the participant preference rating. Participants rated C as their most preferred method, followed by B and then A. The differences across all combinations of A, B, and C in preference rating was significant.

5.1.3 Debriefing

In the debriefing session, participants said that they preferred B and C over A because just relying on the perception of the size of the glyph to estimate the magnitude of the principal stresses was challenging. The additional colormap for the continuous range of principal stress values on B and C instead of binary colors on A helped them in determining the principal stresses more accurately. Some participants reported that the gradient of colors on B and C further assisted them in estimating principal directions. The majority of the participants preferred C the most because of its "simple shape." They found the shape of glyph A and B to be "complex" as the superquadric glyphs took a concave shape for the indefinite tensors. Some participants commented that they did not find it necessary to highlight indefinite tensors through this change in shape. Many participants said because of the "simple shape" of C it was

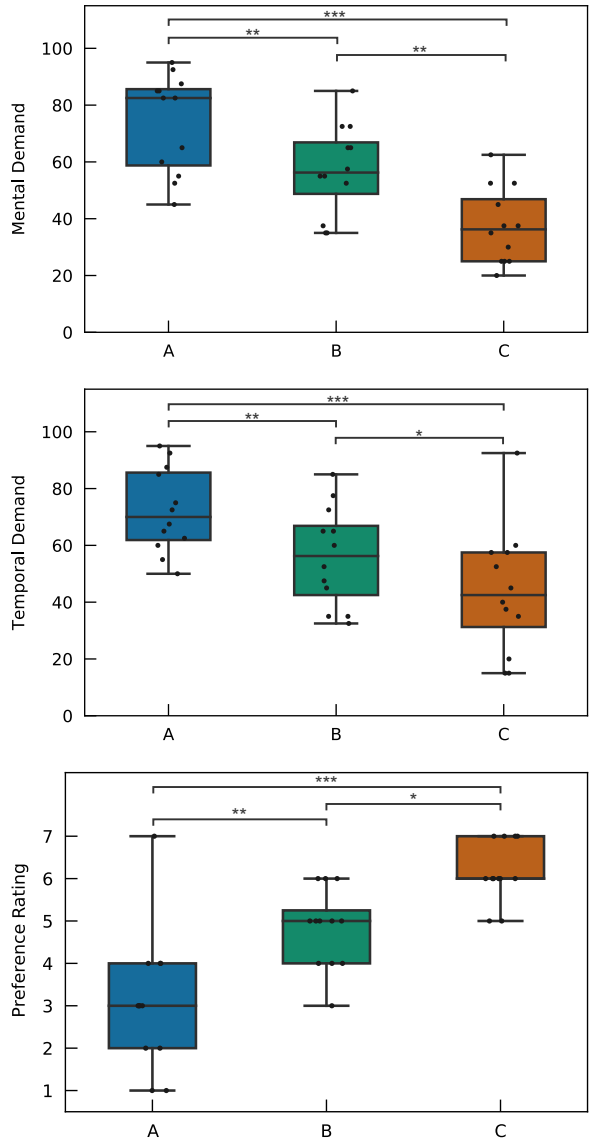

Fig. 6. Subjective user feedback on the glyph designs. *Top:* Mental demand in determining the state of stress across all the glyph designs. *Middle:* Temporal demand in determining the state of stress across all the glyph designs. *Bottom:* User preference rating in determining the state of stress for the glyph designs. The symbols *, **, and *** indicate p value $<$0.05, $<$0.01 and $<$0.001 for pairwise Student-Newman-Keuls post hoc test.

easier to learn C compared to A and B. Few users found that the "pointy feature" of glyph A and B for indefinite tensors helped in better estimating the principal directions compared to the "convex or rounded shape" of C. Two users suggested that having a glyph with a similar "pointy features" of extended SQ glyph along all the principal directions will be better in estimating all the principal directions than the "convex shape" of glyph C.

5.2 Glyph placement

In this section, we compare the user accuracy and subjective user feedback for two glyph placement strategies coupled with two different glyphs A and C to visualize stresses and displacements in a 3D space. Here we compare glyph placement strategy of placing stress tensor glyphs on displacement streamlines against a baseline of placing glyphs on a 3D Cartesian grid. As before, in the graphs and discussion, we use the following abbreviations for the methods: *AG*: Glyph A on a 3D grid; *CG* Glyph C on a 3D grid; *AS* Glyph A on displacement streamline, *CS* Glyph C on displacement streamline. Table 2 shows the statistics for the glyph placement visualization methods comparisons.

TABLE 2
Statistics for glyph placement visualization method comparisons. DOF is the degree of freedoms in the χ^2 statistic.

Comparison across all glyph placement methods	F	χ^2	p
Mean stress insights error	24.7	-	$<$0.001
Median principal direction error	-	15.6; 3 DOF	$<$0.001
Median mental demand	-	22.0; 3 DOF	$<$0.001
Mean temporal demand	9.6	-	$<$0.001
Mean user preference rating	12.7	-	$<$0.001

5.2.1 Quantitative summary

The user stress insight errors were significantly lower for *CG* and *CS* compared to *AG* and *AS* (see Figure 7). The results align with prior findings that users had better accuracy in determining stress with C compared to A. While just comparing glyph placement strategy for both A and C, users had lower stress insight errors when glyphs were placed on displacement streamlines, but the differences were not statistically significant.

All the visualization methods used the same glyphs to represent local displacement. The only difference across visualization methods for displacement glyph was their placement strategy. Users had significantly lower displacement insight errors when the glyphs were placed on displacement streamline for *AS* and *CS* compared to a 3D Cartesian grid for *AG* and *CG* (see Figure 7).

5.2.2 Subjective summary

Participants ranked *CS* to have the lowest mental and temporal demand, which was significantly lower compared to all the other methods in visualizing the stress and displacements fields in a 3D space (see Figure 8). We found no significant difference in mental demand among all the other methods. *CG* had significantly lower temporal demand compared to *AG*. We found no significant difference between *AG* and *CG* compared to *AS*. *CS* was the most user preferred method. The preference for *CS* was significantly higher than all the other methods. Among the other methods, *CG* was significantly more preferred than *AG*. Furthermore, most users also agreed that visualizing displacements along with stress helped in visualizing the trends in stress tensor fields.

5.2.3 Debriefing

In the debriefing session, the majority of the users reported that they preferred placing glyphs on displacement streamlines as it allowed them to better visualize displacement fields, which in turn intuitively helped them to understand the underlying stress fields. Few users commented that placing glyphs on displacement streamlines made the whole visualization more aesthetically pleasing. Some participants said that they experienced loss of relative position and

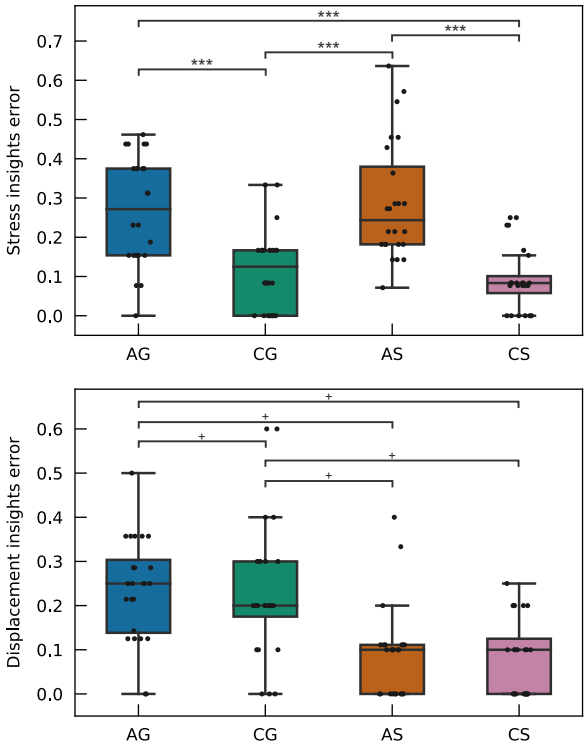

Fig. 7. Quantitative user error in estimating stress and displacement fields in 3D space. *Top:* User stress insight errors across all visualization methods *Bottom:* User displacement insights error across all visualization methods. The symbols + and *** indicate p values of <0.05 and <0.001 for pairwise Student-Newman-Keuls post hoc test.

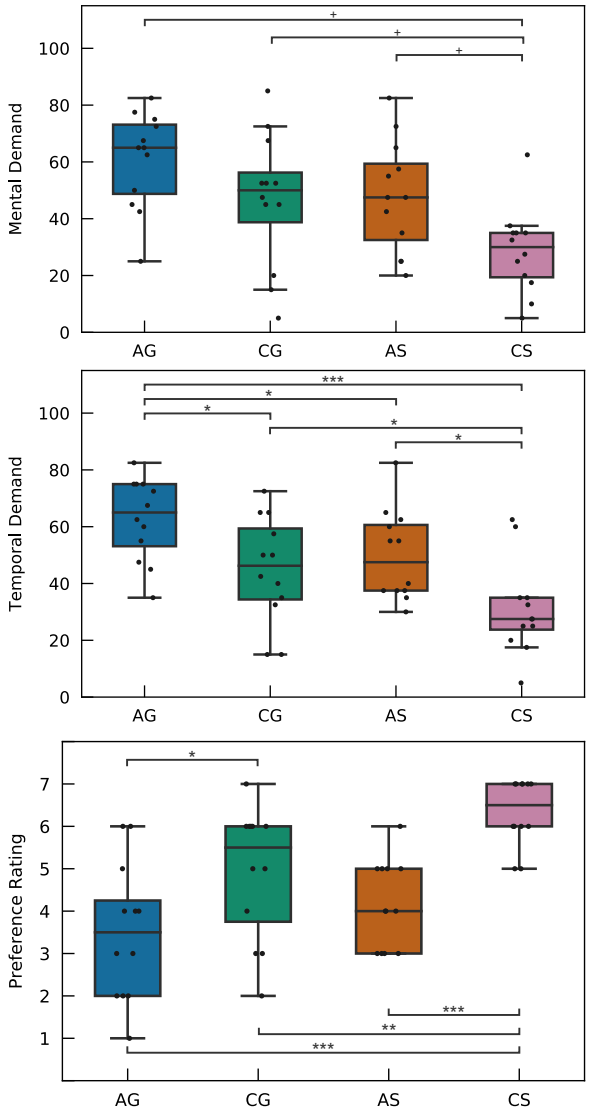

Fig. 8. Subjective user feedback on the visualization methods. *Top:* Mental demand in understanding the stress and displacement fields across all methods. *Middle:* Temporal demand in understanding the stress and displacement fields across all methods. *Bottom:* User preference rating in understanding the stress and displacements fields across all methods. The symbols +, *, **, and *** indicate p values of <0.05, <0.05, <0.01 and <0.001 for pairwise Student-Newman-Keuls post hoc test.

orientation with placing glyphs on a 3D Cartesian grid, as the visualization looked similar from different angles.

Many participants said that they preferred C over A as it was easier to estimate stress magnitude more easily from the colormap of C rather than just the size of glyph A. Some user said that while the VR experience and the ability to look at glyph A from different angles allowed them to estimate the stress magnitude better, it still required more time than C. Several participants said that they found that A looked smaller when it took the concave shape for indefinite stress tensor, which created a perceptual asymmetry between indefinite tensor, and positive and negative-definite tensors.

In their daily workflow, the majority of the participants graphed contour plots of line plots of individual stress components to visualize the stress field. Most of the participants found that *CS* was an improvement over their current visualization method. However, few participants added that *CS* was more appropriate for a general overall exploratory analysis of the stress field. For a more in-depth understanding of the stress field, particularly in cases of high spatial frequency changes in the stress field, they see more value in line plots and contour plots of individual stress components in that local region. Several users reported that they preferred experiencing the visualization in VR over a desktop screen as it allowed them to be inside the 3D space of the visualization. Few participants said having the stress visualization with the VR experience integrated with their every day finite-element analysis software would be crucial in the adoption of the visualization technique in their daily workflow.

5.2.4 *Pilot studies*

In our pilot studies, we explored various glyph placement strategies. We examined glyph placement on tensorlines along a one principal direction field. This strategy worked well for tensor fields with one major principal stress but did not generalize effectively for other cases. We also investigated placing glyphs on hyperstreamlines, which incorporate principal stress and principal directions along the tensorline. But this method was limited to a very low resolution because of clutter in 3D space. We also explored placing glyphs on points generated by anisotropic dart throwing with glyph separation distance based on scalar quantities like stress magnitude or von Mises stress. This strategy allowed for sparse glyph placement avoiding clutter, but

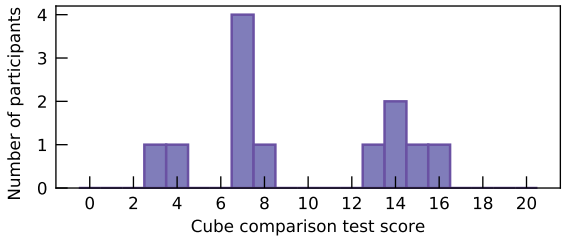

Fig. 9. Distribution of participant scores on the cube comparison test to evaluate mental rotation ability.

it failed at showing the underlying continuous structure in the tensor field.

5.3 Between-group differences

5.3.1 High vs. low mental rotation ability

The distribution of participants' scores on the cube comparison test to assess their mental rotation ability is shown in Figure 9. We looked for between-group differences based on the cube comparison test scores to check if higher quantitative errors for glyph and glyph placement trials correlated with lower cube comparison scores. For this comparison, we used a threshold of 10 points to divide participants into two groups. The participant group with scores of more than 10 points were considered to have high mental rotation ability compared to the group, that scored less than 10 points. We examined these between-group differences for every error metric for each visualization method in the glyph and glyph placement trials. Among all the comparisons, only for glyph B did we observe that the group with higher mental rotation scores had significantly lower ($p = 0.002$) eigenvector errors compared to the group with lower mental rotation scores. While we did not find a significant correlation between mental rotation scores and the effectiveness of the visualization, that is not evidence for no correlation. A future study with more participants or trials might find a significant correlation.

5.3.2 Novice vs. Expert

We classified the two undergraduate and the ten doctoral student participants as novices and experts respectively. We found no evident pattern between novices and experts in the error metrics for all the visualization method in each of the glyph and glyph placement trials.

6 Discussion

6.1 Glyph user study

While both glyphs B and C had the highest objective accuracy scores, in the subjective feedback C performed the best. The results aligned with our hypothesis. User comments validated our design idea that a colormap coupled with the size of a glyph gives the best estimation of the principal stresses. The relatively simple shape of C also contributed to the higher user preference rating. A limitation of C is that its color encoding leads to artificial highlighting of principal directions, which may be irrelevant for nearly isotropic tensor cases.

Despite the same shape, B had higher accuracy than A on the estimation of principal direction, suggesting that using a gradient of color to represent principal stresses on the glyph improves the user perception of the shape and orientation of the glyph.

The limitation of the glyph accuracy tests are task complexity in the selection of principal directions and restricting participants to only view the glyph from one viewpoint. However, accuracy tests aimed at comparing the various glyph designs, not to obtain absolute errors associated with glyph perception. Additionally, Schultz et al. [18] also had the halos around glyph A to improve the glyph visibility even as eigenvalues get close to zero. In our evaluation, owing to the incapability of Matlab's visualization toolbox to generate halos, in our trial, A was evaluated without the halos. However, as only 14.8% of cases in our glyph evaluation trial had eigenvalues near zero, i.e., having an absolute value less than 0.2, we hypothesize that the omission of halos would not have a significant impact on the relative performance of the various glyphs in our user trial. To be certain, this would need to be tested in a future experiments. Additionally, in the future, halos could be included in our proposed glyph C to address the issue of eigenvalues getting close to zero and possibly improve the overall aesthetics and glyph shape perception.

6.2 Glyph placement user study

Overall, *CS* performed the best in the stress and displacement insight errors, and subjective user rating. Glyph placements on displacement streamlines had similar stress insight errors and, as expected, significantly lower displacement insight errors for both glyphs A and C. However, in most of the subjective user metrics, glyph placements on displacement streamlines performed the best for both A and C. When comparing A and C, again as previous results indicated, C performed significantly better in stress insight errors and the subjective user metrics. A difference to note is that the glyph accuracy tests performed in the Matlab GUI used orthographic projection, while the glyph placement tests in VR used perspective projection.

Designing a user task to evaluate user understanding of a tensor field was challenging. We created the user trial considering the most typical analysis applications in mechanical engineering, where experts are searching for regions of stress concentrations or high-stress values and also variations of tensor fields. It is also true that many mechanical analysis applications do not require searching high-stress regions. But coming up with user tasks which evaluate and encompass needs of the weird variety of mechanical analysis is not trivial. While it can also be pointed out that if the mechanical analysis task required identifying regions of large stress concentration, such regions could be highlighted instead of asking users to search for these regions. However, the fact that users could identify high-stress value regions indicates to some extent that the users were able to explore and understand the tensor fields in the user tasks. Thus, owing to the nature of the trial, we believe that while stress insight errors are useful in making comparisons between methods, they do not provide a complete evaluation of methods. Instead, subjective user metrics and comments

offer a significant measure of the overall effectiveness and usefulness of the visualization method.

In our method, we visualized the stress tensor and the displacement vector fields at the same time. The participant feedback showed that the visualization of the displacement field assisted them in understanding the tensor field. However, if required, the displacement glyph can always be dropped from the visualization.

The trial only tested two tensor field datasets for each method because the study design was already about 2 hours long and any additional testing of another tensor field would have made the study prohibitively long to recruit participants.

6.3 Glyph color encoding

The goal of our color encoding is to distinguish the sign of the principal stress, encode the value of the principal stress, and to improve the user estimation of the principal stress direction. Instead of uniform colors for each principal direction, our color encoding generates a gradient of color. The color saturation decreases as a quartic function of the distance to ensure a large region of the glyph had the color match with the principal stress value both in sign and magnitude from the colormap. Utilizing a simple diverging colormap would not result in such a color encoding scheme. Furthermore, the principal stress magnitude is dually encoded both from the size and the color of the glyph. The quartic function of the color saturation also ensures only a small region on the glyph had a strong gradient, which was aimed at improving principal direction estimation.

Similar color gradient effects can also be achieved using angular subdivision from the principal directions instead of the distance computations. While we investigated utilizing angular subdivisions, our results from the distance computations looked more aesthetically pleasing and satisfied our design goals. However, in future studies, approaches utilizing angular subdivisions for color encoding can be explored.

The shading and highlights added to the glyph improve the 3D perception of the glyph geometry, which, in turn, aids the user estimation of the principal stress magnitude from the size of the glyph. At the same time, the shading and highlights on the glyph also impede the ability to accurately evaluate the glyph color and its corresponding principal stress value from the colormap. Thus, there is a delicate balance in the use of shading, and it needs to be customized according to the display medium being utilized. While the lighting conditions can be improved further, such improvements will affect all the glyphs, and it should not change the relative performance of the glyphs.

Lastly, estimating the principal stresses from the glyph's color and geometry was more challenging in the glyph user study because the users were not allowed to alter the viewpoint from which they were observing the glyph. However, this task did become more effortless in the glyph placement study where the users in VR could change their view from which they were observing the glyph. Furthermore, in the presence of multiple glyphs in the visualization, the neighboring glyphs can be used to compare the relative changes in the color, size and shape of the glyphs; so the trends in the stress tensor field can be more easily observed.

6.4 Virtual reality as display medium

In the glyph placement user trial, we used VR as the mode of the display because multiple glyphs-based tensor field visualization is highly information dense. Each glyph through its shape, size, and color represents a six-dimensional tensor quantity placed in a 3D space. The immersive experience of VR increases the capability to gauge the 3D cues in the visualization, thus achieving a more accurate perception of the tensor field. Therefore, to evaluate and compare visualization at their most effectiveness, we utilized VR as the mode of display in the glyph placement study. In comparison, we expect all the visualizations to have reduced performance in a desktop setting. However, we hypothesise that rankings of the visualizations may well stay the same in 2D displays because many of the relevant 3D visual characteristics will also be relevant in 2D displays. But further studies would be required to compare the effectiveness of the visualizations on 2D displays conclusively.

6.5 Scalability

Using our method, the visualization of stress tensor fields varying with high spatial frequency would require very dense sampling of the tensor glyphs. While this is technically possible, perceptually having too many glyphs leads to occlusion and clutter in visualization and would make it hard for the user to see the underlying continuous structures in the tensor fields. Thus, our approach is limited to visualizing low spatial frequency stress fields. Future studies could explore interactive approaches for the visualization of high-spatial frequency stress fields, where, in the zoomed-out state low spatial frequency content of the stress field is visualized, and on zooming in on a particular region, the higher spatial frequency content of the stress field is visualized.

In this study, we did not explore the computational performance limitation of the visualization with too many glyphs. In user trials, our visualizations had up to 958 glyphs, and a standard VR capable laptop was able to render it with ease. In these visualizations, we used 1860 vertices and 3416 faces to achieve the dense coloring of the glyphs. However, the color and triangulations can be sampled more sparsely to reduce the computational cost of the visualization.

7 Conclusion

In this paper, we present an adaptation of design strategies for glyph-based visualizations for 3D stress tensor fields. We also conduct formal user studies to evaluate various glyph based tensor visualization methods. The results of user studies with domain experts show that the use of red-blue encoded SQ glyph (glyph C) most effectively and accurately showed all the components of the stress tensor at a discrete location. Moreover, by combining glyph C with glyph placement on displacement streamlines (*CS*), users could observe the continuous internal structures in the 3D tensor field. Another contribution of our method is that it can show both the displacement and stress tensor fields in the same visualization. Using our visualization method, experts can gain insights and intuitions of stress

tensor fields to solve various problems with applications in mechanical engineering. We also summarized the design lessons learned through user studies with domain experts. This information could be useful in guiding the development of further useful stress tensor field visualizations.

ACKNOWLEDGMENT

We acknowledge funding from the Graduate School, Brown University. We wish to thank Johannes Novotny and Alexander K Landauer for the helpful discussions, and Brandon Li for helping develop the interaction capability in Unity. Part of this research was conducted using the computational resources and services at the Center for Computation and Visualization, Brown University.

REFERENCES

[1] F. Yc and Y. Fung, "Foundations of solid mechanics," 1965.
[2] C. Dick, J. Georgii, R. Burgkart, and R. Westermann, "Stress tensor field visualization for implant planning in orthopedics," *IEEE Transactions on Visualization and Computer Graphics*, vol. 15, no. 6, pp. 1399–1406, 2009.
[3] J. Toyjanova, E. Bar-Kochba, C. López-Fagundo, J. Reichner, D. Hoffman-Kim, and C. Franck, "High resolution, large deformation 3d traction force microscopy," *PloS one*, vol. 9, no. 4, p. e90976, 2014.
[4] Y. M. Hashash, J. I.-C. Yao, and D. C. Wotring, "Glyph and hyperstreamline representation of stress and strain tensors and material constitutive response," *International journal for numerical and analytical methods in geomechanics*, vol. 27, no. 7, pp. 603–626, 2003.
[5] W. D. Callister and D. G. Rethwisch, *Materials science and engineering*. John Wiley & Sons NY, 2011, vol. 5.
[6] A. Kratz, C. Auer, and I. Hotz, "Tensor invariants and glyph design," in *Visualization and Processing of Tensors and Higher Order Descriptors for Multi-Valued Data*. Springer, 2014, pp. 17–34.
[7] I. Hotz, L. Feng, H. Hagen, B. Hamann, K. Joy, and B. Jeremic, "Physically based methods for tensor field visualization," in *Proceedings of the conference on Visualization'04*. IEEE Computer Society, 2004, pp. 123–130.
[8] A. Kratz, C. Auer, M. Stommel, and I. Hotz, "Visualization and analysis of second-order tensors: Moving beyond the symmetric positive-definite case," in *Computer Graphics Forum*, vol. 32, no. 1. Wiley Online Library, 2013, pp. 49–74.
[9] A. Maries, A. Haque, S. L. Yilmaz, M. B. Nik, and G. E. Marai, "Interactive exploration of stress tensors used in computational turbulent combustion," in *New Developments in the Visualization and Processing of Tensor Fields*. Springer, 2012, pp. 137–156.
[10] A. Maries, T. Luciani, P. H. Pisciuneri, M. B. Nik, S. L. Yilmaz, P. Givi, and G. E. Marai, "A clustering method for identifying regions of interest in turbulent combustion tensor fields," in *Visualization and Processing of Higher Order Descriptors for Multi-Valued Data*. Springer, 2015, pp. 323–338.
[11] G. E. Marai, T. Luciani, A. Maries, S. L. Yilmaz, and M. B. Nik, "Visual descriptors for dense tensor fields in computational turbulent combustion: a case study," *Electronic Imaging*, vol. 2016, no. 1, pp. 1–11, 2016.
[12] Y. Masutani, S. Aoki, O. Abe, N. Hayashi, and K. Otomo, "Mr diffusion tensor imaging: recent advance and new techniques for diffusion tensor visualization," *European journal of radiology*, vol. 46, no. 1, pp. 53–66, 2003.
[13] A. Kratz, B. Meyer, and I. Hotz, "A visual approach to analysis of stress tensor fields," in *Dagstuhl Follow-Ups*, vol. 2. Schloss Dagstuhl-Leibniz-Zentrum für Informatik, 2011.
[14] C. Zhang, T. Schultz, K. Lawonn, E. Eisemann, and A. Vilanova, "Glyph-based comparative visualization for diffusion tensor fields," *IEEE transactions on visualization and computer graphics*, vol. 22, no. 1, pp. 797–806, 2015.
[15] T. Jankun-Kelly, Y. Lanka, and J. Swan, "An evaluation of glyph perception for real symmetric traceless tensor properties," in *Computer Graphics Forum*, vol. 29, no. 3. Wiley Online Library, 2010, pp. 1133–1142.
[16] M. Meuschke, S. Voß, O. Beuing, B. Preim, and K. Lawonn, "Glyph-based comparative stress tensor visualization in cerebral aneurysms," in *Computer Graphics Forum*, vol. 36, no. 3. Wiley Online Library, 2017, pp. 99–108.
[17] G. Kindlmann, "Superquadric tensor glyphs," in *Proceedings of the Sixth Joint Eurographics-IEEE TCVG conference on Visualization*. Eurographics Association, 2004, pp. 147–154.
[18] T. Schultz and G. L. Kindlmann, "Superquadric glyphs for symmetric second-order tensors," *IEEE transactions on visualization and computer graphics*, vol. 16, no. 6, pp. 1595–1604, 2010.
[19] A. Abbasloo, V. Wiens, M. Hermann, and T. Schultz, "Visualizing tensor normal distributions at multiple levels of detail," *IEEE transactions on visualization and computer graphics*, vol. 22, no. 1, pp. 975–984, 2015.
[20] R. B. Haber, "Visualization techniques for engineering mechanics," *Computing Systems in Engineering*, vol. 1, no. 1, pp. 37–50, 1990.
[21] J. G. Moore, S. A. Schorn, and J. Moore, "Methods of classical mechanics applied to turbulence stresses in a tip leakage vortex," in *ASME 1995 International Gas Turbine and Aeroengine Congress and Exposition*. American Society of Mechanical Engineers, 1995, pp. V005T16A006–V005T16A006.
[22] R. Kriz, M. Yaman, M. Harting, and A. Ray, "Visualization of zeroth, second, fourth, higher order tensors, and invariance of tensor equations," *Computers and Graphics*, vol. 21, no. 6, pp. 1–13, 2005.
[23] T. Gerrits, C. Rössl, and H. Theisel, "Glyphs for general second-order 2d and 3d tensors," *IEEE transactions on visualization and computer graphics*, vol. 23, no. 1, pp. 980–989, 2016.
[24] K. Shimada, A. Yamada, T. Itoh *et al.*, "Anisotropic triangular meshing of parametric surfaces via close packing of ellipsoidal bubbles," in *6th International Meshing Roundtable*, 1997, pp. 375–390.
[25] G. Kindlmann and C.-F. Westin, "Diffusion tensor visualization with glyph packing," *IEEE Transactions on Visualization and Computer Graphics*, vol. 12, no. 5, 2006.
[26] S. B. Vos, M. A. Viergever, and A. Leemans, "Multi-fiber tractography visualizations for diffusion mri data," *PloS one*, vol. 8, no. 11, p. e81453, 2013.
[27] V. Prckovska, T. H. Peeters, M. van Almsick, B. ter Haar Romeny, and A. V. i Bartroli, "Fused dti/hardi visualization," *IEEE Transactions on Visualization and Computer Graphics*, vol. 17, no. 10, pp. 1407–1419, 2010.
[28] M. Hlawitschka, G. Scheuermann, and B. Hamann, "Interactive glyph placement for tensor fields," in *International Symposium on Visual Computing*. Springer, 2007, pp. 331–340.
[29] A. Kratz, N. Kettlitz, and I. Hotz, "Particle-based anisotropic sampling for two-dimensional tensor field visualization," 2011.
[30] L. Feng, I. Hotz, B. Hamann, and K. Joy, "Anisotropic noise samples," *IEEE Transactions on Visualization and Computer Graphics*, vol. 14, no. 2, pp. 342–354, 2008.
[31] A. Vilanova, S. Zhang, G. Kindlmann, and D. Laidlaw, "An introduction to visualization of diffusion tensor imaging and its applications," in *Visualization and Processing of Tensor Fields*. Springer, 2006, pp. 121–153.
[32] D. Weinstein, G. Kindlmann, and E. Lundberg, "Tensorlines: Advection-diffusion based propagation through diffusion tensor fields," in *Proceedings of the conference on Visualization'99: celebrating ten years*. IEEE Computer Society Press, 1999, pp. 249–253.
[33] T. Schultz and A. Vilanova, "Diffusion mri visualization," *NMR in Biomedicine*, vol. 32, no. 4, p. e3902, 2019.
[34] T. Delmarcelle and L. Hesselink, "Visualization of second order tensor fields and matrix data," in *Proceedings of the 3rd conference on Visualization'92*. IEEE Computer Society Press, 1992, pp. 316–323.
[35] T. Delmarcelle and Hesselink, "Visualizing second-order tensor fields with hyperstreamlines," *IEEE Computer Graphics and Applications*, vol. 13, no. 4, pp. 25–33, 1993.
[36] G. Scheuermann, J. Frey, H. Hagen, B. Hamann, B. Jeremic, and K. I. Joy, "Visualization of seismic soils structure interaction simulations." in *VIIP*, 2001, pp. 78–83.
[37] V. Wiens, L. Schlaffke, T. Schmidt-Wilcke, and T. Schultz, "Visualizing uncertainty in hardi tractography using superquadric streamtubes," in *Proc. EG Conf. on Visualization (EuroVis) Short Papers*, 2014.
[38] T. Schultz and G. Kindlmann, "A maximum enhancing higher-order tensor glyph," in *Computer Graphics Forum*, vol. 29, no. 3. Wiley Online Library, 2010, pp. 1143–1152.

[39] S. G. Hart and L. E. Staveland, "Development of nasa-tlx (task load index): Results of empirical and theoretical research," in *Advances in psychology*. Elsevier, 1988, vol. 52, pp. 139–183.
[40] R. Likert, "A technique for the measurement of attitudes." *Archives of psychology*, 1932.
[41] C. North, "Toward measuring visualization insight," *IEEE computer graphics and applications*, vol. 26, no. 3, pp. 6–9, 2006.
[42] J. D. Eshelby, "The determination of the elastic field of an ellipsoidal inclusion, and related problems," *Proc. R. Soc. Lond. A*, vol. 241, no. 1226, pp. 376–396, 1957.
[43] J. Eshelby, "The elastic field outside an ellipsoidal inclusion," *Proc. R. Soc. Lond. A*, vol. 252, no. 1271, pp. 561–569, 1959.
[44] R. B. Ekstrom, J. W. French, H. Harman, and D. Derman, *Kit of factor-referenced cognitive tests*. Princeton, NJ: Educational Testing Service, 1976.

Mohak Patel received his BTech degree in mechanical engineering from Indian Institute of Technology, Gandhinagar in 2013. He is currently working on the PhD degree in engineering and the Sc.M degree in computer science from Brown University. His research interests include cell mechanics, motion tracking algorithms, visualization, machine learning and computer vision.

David H. Laidlaw received the PhD degree in computer science from the California Institute of Technology, where he also did post-doctoral work in the Division of Biology. He is a professor in the Computer Science Department, Brown University. His research centers on applications of visualization, modeling, computer graphics, and computer science to other scientific disciplines. He is a fellow of the IEEE.